Supplemental Material
Stochastic Snowball States in Planetary Climate

Duc Thach Son Vu[a], John S. Wettlaufer[b,c,*]

[a] *Department of Earth & Planetary Sciences, Yale University, New Haven, CT 06511, USA*
[b] *Departments of Earth & Planetary Sciences, Mathematics and Physics, Yale University, New Haven, CT 06511, USA*
[c] *Nordita, KTH Royal Institute of Technology and Stockholm University, SE-106 91, Stockholm, Sweden*

Here we provide a quantitative argument for the high-frequency fluctuations in eccentricity based on circumbinary planets Kepler-16b, Kepler-34b and Kepler-35b. We then collect additional figures to supplement the main text.

Eccentricity Fluctuations of Circumbinary Planets

Using the values in Table 2 of Leung and Lee (2013), particularly the *apsidal*, *guiding-center* and *epicyclic or free eccentricity* frequencies, we discuss the origin of high frequency, or short period, osculating eccentricity as seen in their Figures 1, 4, 5 and 7.

Leung and Lee (2013) represent the planetary motion by superposing the circular motion of a guiding center, the forced oscillations, originating in the non-axisymmetric components of the binary's potential, the epicyclic and vertical motions.

We determine the frequencies n_0 and κ_0 (apsidal), n_0 and ν_0 (nodal), using the values in their Table 2 of the Keplerian mean frequency $n_K = \mathrm{yr}^{-1}$, and the ratios n_0/n_K, κ_0/n_K and ν_0/n_K viz.

$$n_0 = \left(\frac{n_0}{n_K}\right) n_K \qquad \text{and} \qquad \kappa_0 = \left(\frac{\kappa_0}{n_K}\right) n_K \qquad \text{and} \qquad \nu_0 = \left(\frac{\nu_0}{n_K}\right) n_K,$$

to calculate the guiding center, epicyclic or free eccentricity, and apsidal periods, P_0, P_κ and P_{aps} respectively, for Kepler-16 b, 34 b, 35 b as follows.

Relevant periods for Kepler-16 b.

(1) Guiding-center period:

$$P_0 = \frac{2\pi}{n_0} \approx \frac{2\pi}{10.1531} \approx 0.619 \text{ yr} \approx 226 \text{ days}. \tag{0.1}$$

(2) Epicyclic/free-eccentricity period:

$$P_\kappa = \frac{2\pi}{\kappa_0} \approx \frac{2\pi}{10.0041} \approx 0.628 \text{ yr} \approx 229 \text{ days} \tag{0.2}$$

*Corresponding author: john.wettlaufer@yale.edu, jw@fysik.su.se
Email addresses: ducthachson.vu@yale.edu (Duc Thach Son Vu), john.wettlaufer@yale.edu, jw@fysik.su.se (John S. Wettlaufer)

(3) Apsidal (beat) period:

$$P_{\rm aps} = \frac{2\pi}{|n_0 - \kappa_0|} \approx \frac{2\pi}{0.1490} \approx 42.2 \text{ yr.} \tag{0.3}$$

Relevant periods for Kepler-34 b.

Using

$$n_0 = 8.0512 \times 1.00423 \approx 8.0853 \text{ yr}^{-1}, \qquad \kappa_0 = 8.0512 \times 0.99567 \approx 8.0163 \text{ yr}^{-1}.$$

(1) Guiding-center period:

$$P_0 \approx \frac{2\pi}{8.0853} \approx 0.777 \text{ yr} \approx 284 \text{ days}, \tag{0.4}$$

(2) Epicyclic/free-eccentricity period:

$$P_\kappa \approx \frac{2\pi}{8.0163} \approx 0.784 \text{ yr} \approx 286 \text{ days}, \tag{0.5}$$

(3) Apsidal (beat) period:

$$P_{\rm aps} = \frac{2\pi}{|n_0 - \kappa_0|}, \quad |n_0 - \kappa_0| \approx 0.0689 \text{ yr}^{-1}, \quad P_{\rm aps} \approx \frac{2\pi}{0.0689} \approx 91.1 \text{ yr.} \tag{0.6}$$

Relevant periods for Kepler-35 b.

Using

$$n_0 = 17.8875 \times 1.00838 \approx 18.0374 \text{ yr}^{-1}, \qquad \kappa_0 = 17.8875 \times 0.99119 \approx 17.7299 \text{ yr}^{-1}.$$

(1) Guiding-center period:

$$P_0 \approx \frac{2\pi}{18.0374} \approx 0.348 \text{ yr} \approx 127 \text{ days}, \tag{0.7}$$

(2) Epicyclic/free-eccentricity period:

$$P_\kappa \approx \frac{2\pi}{17.7299} \approx 0.354 \text{ yr} \approx 129 \text{ days}, \tag{0.8}$$

(3) Apsidal (beat) period:

$$P_{\rm aps} = \frac{2\pi}{|n_0 - \kappa_0|}, \qquad |n_0 - \kappa_0| \approx 0.3075 \text{ yr}^{-1}, \quad P_{\rm aps} \approx \frac{2\pi}{0.3075} \approx 20.4 \text{ yr.} \tag{0.9}$$

The main point is that the slower apsidal beats

$$P_{\rm aps} \approx 42 \text{ yr}, \ 91 \text{ yr}, \ 20 \text{ yr}, \tag{0.10}$$

control the long term modulation/envelope upon which high frequency fluctuations occur. These dominant fast periods in the solution of Leung and Lee (2013) are P_0 and P_κ . From the above, these are sub-year across Kepler-16 b, 34 b, 35 b:

$$P_0, \ P_\kappa \approx (0.35 \text{ to } 0.78) \text{ yr}, \tag{0.11}$$

so when eccentricity is computed from the instantaneous state (osculating elements), it is natural to observe high frequency eccentricity oscillations on roughly subyear timescales because of beating between n_0 and κ_0, plus any additional forced harmonics.

Additional effects in these and other circumbinary systems (Kepler-38, Kepler-64, Kepler-413) leading to multiple timescale fluctuations include, inter-alia, $p:1$ mean-motion resonances, with the possibility of bounded oscillations, or libration of resonance angles, eccentricity pumping, and chaotic overlap near the inner stability limit, which are more likely for planets sitting close to, or migrating through, these commensurabilities, especially for higher binary eccentricity.

Supplementary Figures

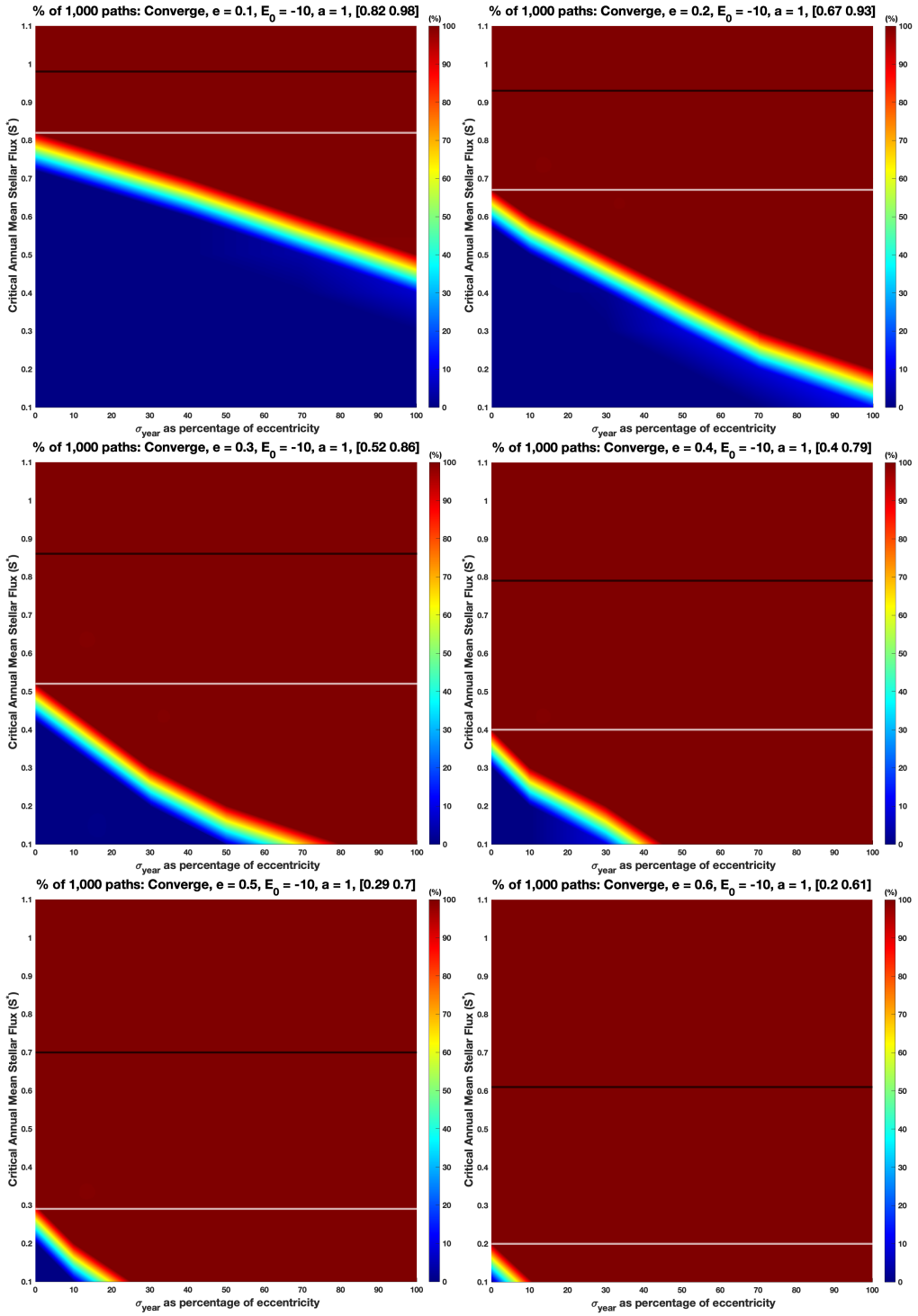


Figure 1: Percentage of 1,000 stochastic paths that converge when $e = 0.1, 0.2, 0.3, 0.4, 0.5, 0.6$ shown as a color map. The two bracketed values in the title of each sub-figure are the critical deterministic values of S^* for convergence and bifurcation given in Table A.2 of the main paper. The white and black horizontal lines are the convergence and bifurcation values respectively.

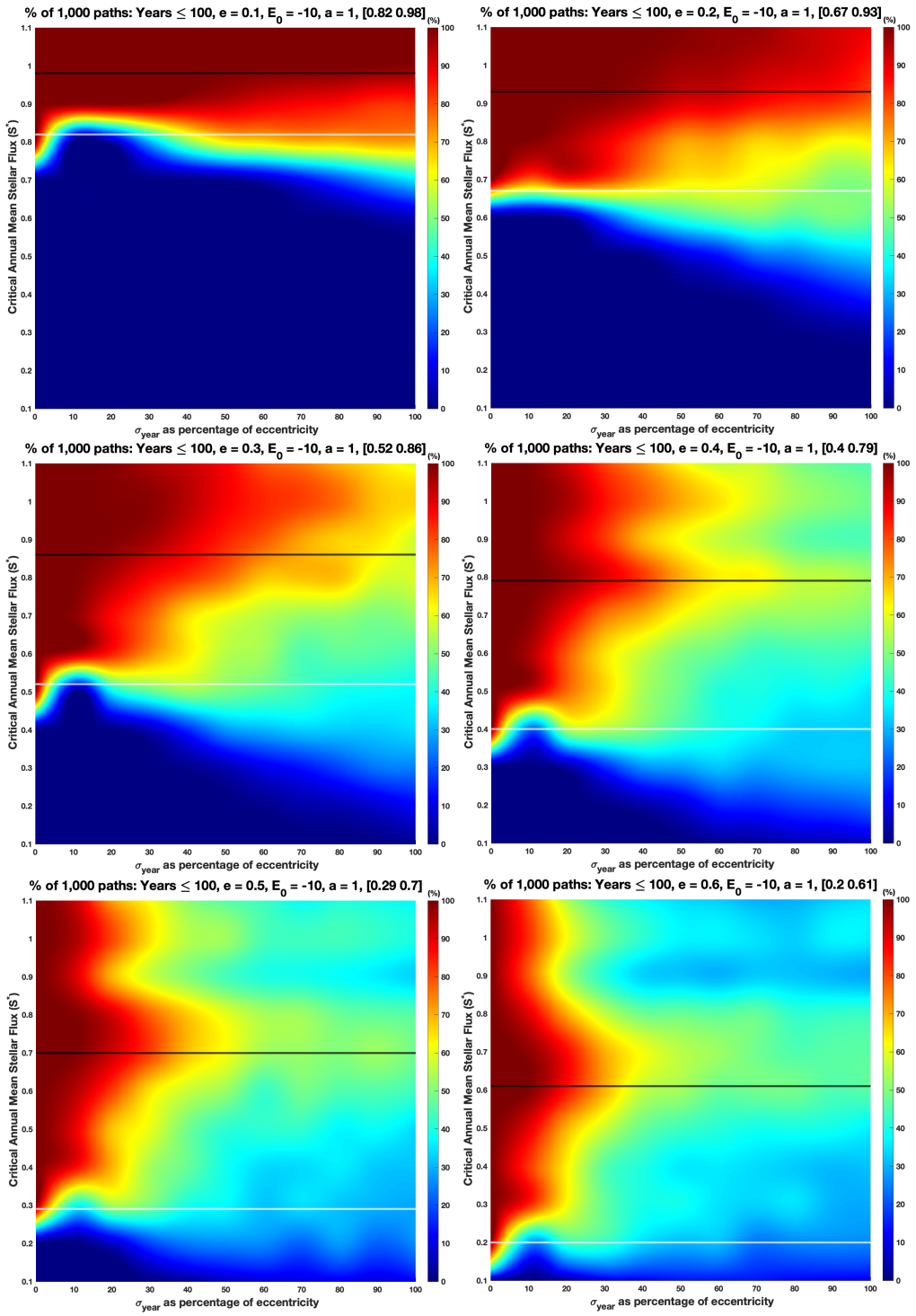


Figure 2: Percentage of 1,000 stochastic paths that converge within 100 years when $e = 0.1, 0.2, 0.3, 0.4, 0.5, 0.6$ shown as a color map. The two bracketed values in the title of each sub-figure are the critical deterministic values of S^* for convergence and bifurcation given in Table A.2 of the main paper. The white and black horizontal lines are the convergence and bifurcation values respectively.

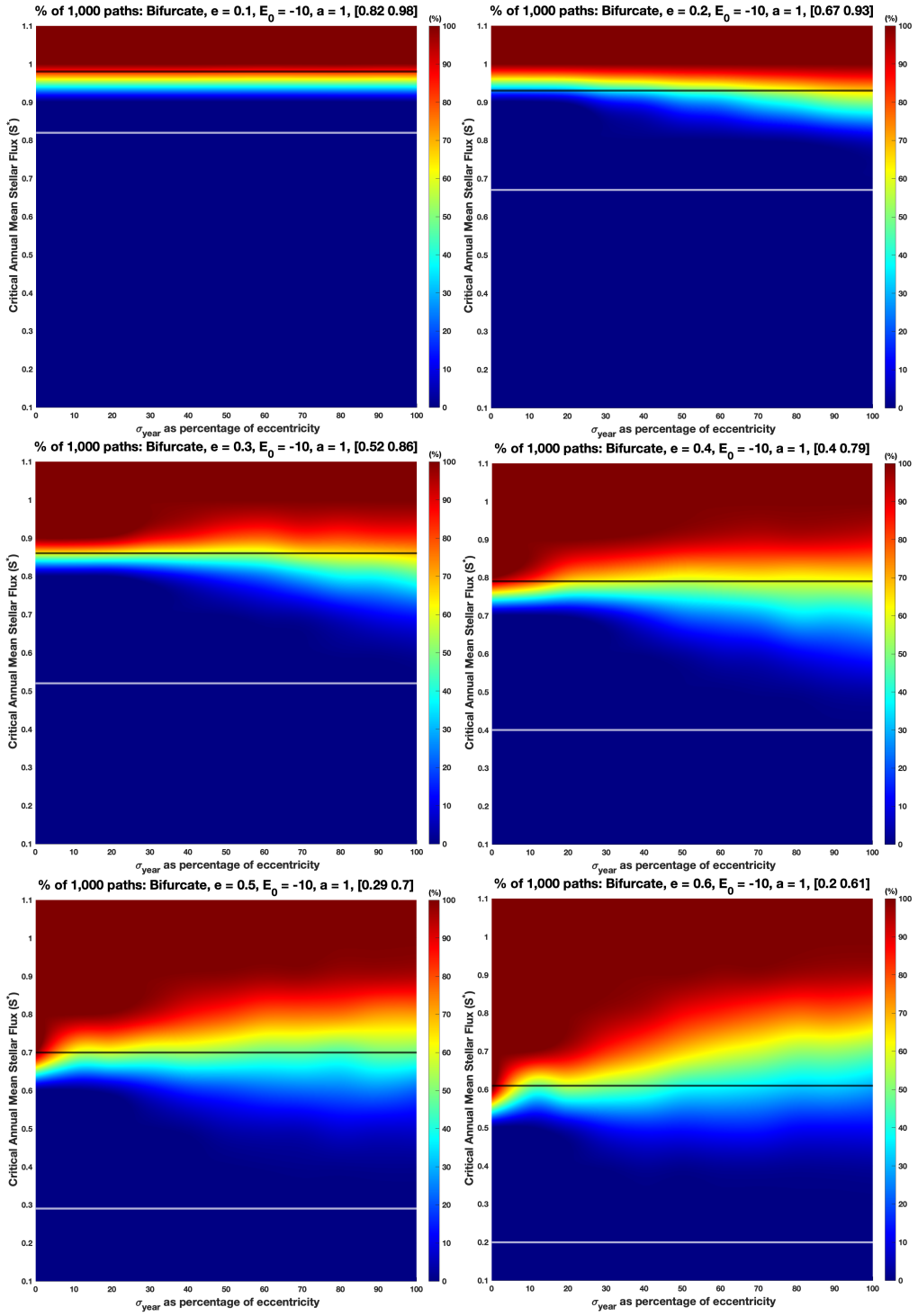


Figure 3: The percentage of bifurcations in 1,000 stochastic paths when $e = 0.1, 0.2, 0.3, 0.4, 0.5, 0.6$ shown as a color map. The two bracketed values in the title of each sub-figure are the critical deterministic values of $S*$ for convergence and bifurcation given in Table A.2 of the main paper. The white and black horizontal lines are the convergence and bifurcation values respectively.

Eccentricity of exoplanets in the NASA database

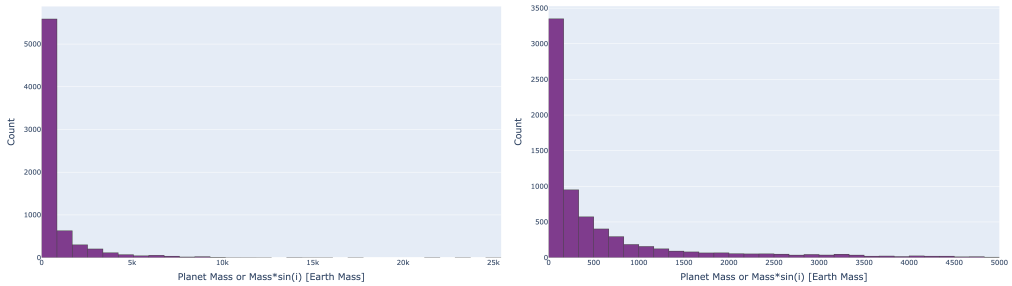


Figure 4: Masses of exoplanets in the NASA (2025) database. The left figure is the histogram of all confirmed exoplanets, and the right figure is the histogram of all exoplanets whose mass is capped at 5000 Earth Masses.

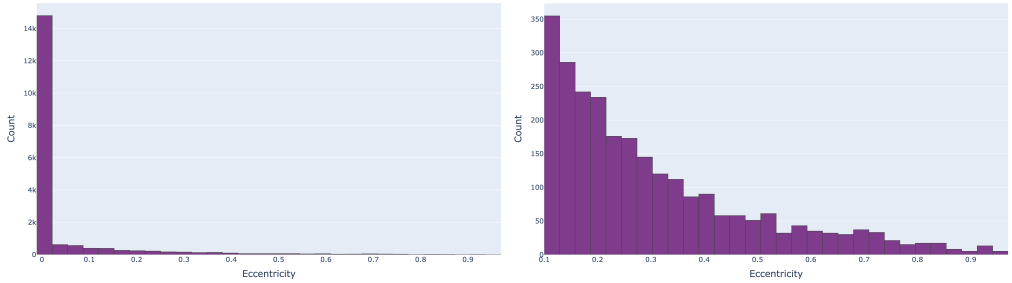


Figure 5: Eccentricities of exoplanets in the NASA (2025) database. The left figure is the histogram of all confirmed exoplanets, and the right figure is the histogram of all exoplanets whose eccentricity is larger than 0.1. For reference, Earth's value is 0.0167.

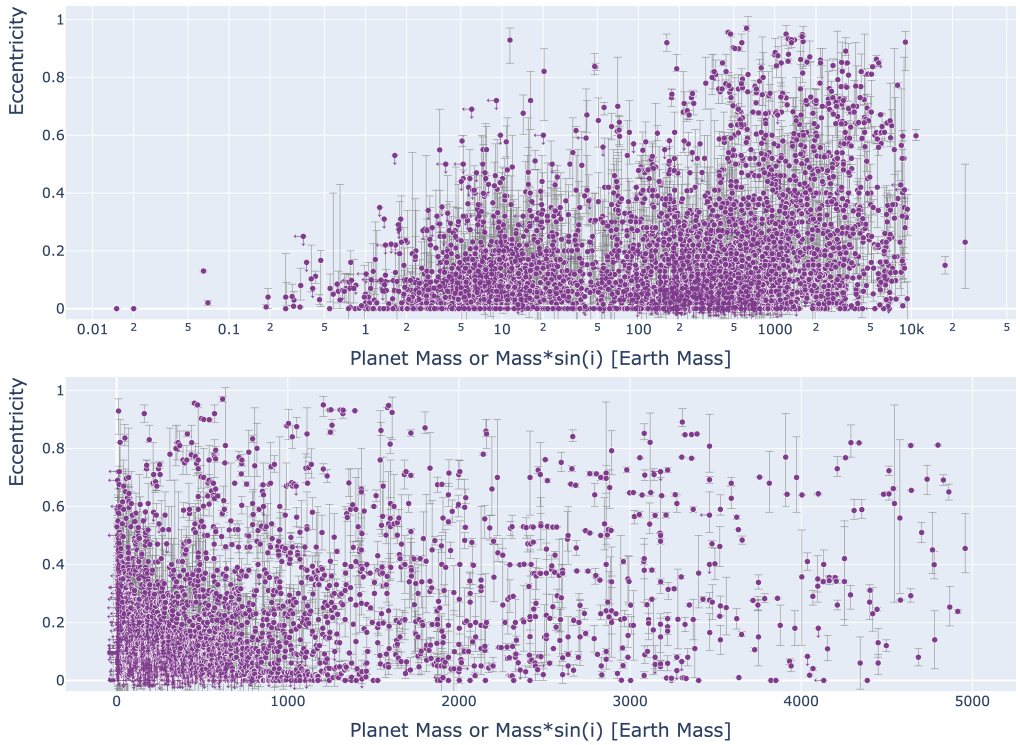


Figure 6: Eccentricity (with error bars for uncertain observations) vs Earth Mass of exoplanets in the NASA (2025) database. The top figure is for all exoplanets, and the bottom is for exoplanets whose mass is capped at 5000 Earth Masses. The horizontal axis in the top figure is scaled in powers of 10, whereas the bottom figure is plotted in a linear scale.

References

G. C. K. Leung, M. H. Lee, An analytic theory for the orbits of circumbinary planets, The Astrophysical Journal 763 (2013) 107. doi:10.1088/0004-637X/763/2/107.

NASA, NASA Exoplanet Archive, 2025. URL: https://exoplanetarchive.ipac.caltech.edu/cgi-bin/TblView/nph-tblView?app=ExoTbls&config=PS. doi:10.26133/NEA12.